View metadata, citation and similar papers at core.ac.uk
brought to you by CORE
provided by NASA Technical Reports Server
Source of Acquisition
NASA Goddard Space Flight Center

Submitted to ApJ

GRB 050717: A Long, Short-Lag Burst Observed by Swift and Konus

H. A. Krimm[1,2], C. Hurkett[3], V. Pal'shin[4], J. P. Norris[1], B. Zhang[5], S. D. Barthelmy[1], D. N. Burrows[6], N. Gehrels[1], S. Golenetskii[4], J. P. Osborne[3], A. M. Parsons[1], M. Perri[7], R. Willingale[3]

krimm@milkyway.gsfc.nasa.gov

December 23, 2005

ABSTRACT

The long burst GRB 050717 was observed simultaneously by the Burst Alert Telescope (BAT) on Swift and the Konus instrument on Wind. Significant hard to soft spectral evolution was seen. Early gamma-ray and X-ray emission was detected by both BAT and the X-Ray Telescope (XRT) on Swift. The XRT continued to observe the burst for 7.1 days and detect it for 1.4 days. The X-ray light curve showed a classic decay pattern including evidence of the onset of the external shock emission at $\sim$ 50 s after the trigger; the afterglow was too faint for a jet break to be detected. No optical, infrared or ultraviolet counterpart was discovered despite deep searches within 14 hours of the burst. The spectral lag for GRB 050717 was determined to be 2.5 $\pm$ 2.6 ms, consistent with zero and unusually short for a long burst. This lag measurement suggests that this burst

[1]NASA Goddard Space Flight Center, Greenbelt, Maryland, 20771, USA

[2]Universities Space Research Association, 10211 Wincopin Circle, Suite 500, Columbia, Maryland 21044-3432, USA

[3]Department of Physics and Astronomy, University of Leicester, Leicester, LE1 7RH, UK

[4]Ioffe Physico-Technical Institute, Laboratory for Experimental Astrophysics, 26 Polytekhnicheskaya, St Petersburg 194021, Russian Federation

[5]Physics Department, University of Nevada, Las Vegas, NV 89154, USA

[6]Department of Astronomy and Astrophysics, 525 Davey Lab., Pennsylvania State University, University Park, PA 16802, USA

[7]ASI Science Data Center, Via Galileo Galilei, I-00044 Frascati, Italy

has a high intrinsic luminosity and hence is at high redshift ($z > 2.7$). GRB 050717 provides a good example of classic prompt and afterglow behavior for a gamma-ray burst.

Subject headings: gamma-ray bursts

1. Introduction

It has been known for many years that spectral evolution operates in long gamma-ray bursts in several ways. Golenetskii et al. (1983) first recognized that the more intense portions of bursts are spectrally harder than the less intense time periods. Concomitantly, individual burst pulses are asymmetric, especially at low energies. This was pointed out by Norris et al. (1996) and later Band (1997) and Norris (2002) showed via spectral lag analysis that, if the burst was bright enough, positive lags were manifest, averaged over the whole time profile. Similarly, and related to the first two effects, the burst "envelope" (containing the peaks and valleys in a burst) tends to soften with time in the vast majority of bursts, an effect that was quantified by Band & Ford (1998). Nemiroff et al. (1994) tied these effects together by demonstrating conclusively that on all time scales, gamma-ray bursts are time-asymmetric. Thus the later, usually lower intensity portions of a burst should also be spectrally softer.

The long gamma-ray burst (GRB) 050717 shows all aspects of these evolutionary trends including overall hard to soft spectral evolution as the prompt emission decays and time asymmetries in all peaks at all energies. Features include two short, soft precursor spikes and at least seven peaks in the main burst.

Norris et al. (1996) also showed that the structure of pulses in GRBs is narrower at high energies. This is another aspect of what Norris et al. (1996) has called the "pulse paradigm," and is physically related to the overall spectral evolution of pulses. In addition, Norris, Marani, & Bonnell (2000) noted that pulse peaks migrate to later times as they become wider at low energies. This spectral lag was found to be proportional to the total peak luminosity of the burst, and can be used to constrain the absolute luminosity and hence the redshift of those bursts, like GRB 050717, for which no spectroscopic redshift was obtained. GRB 050717 was unusual in that its spectral lag is very short (positive but statistically consistent with zero – see Section 4.1), while nearly all long bursts clearly show a large positive spectral lag (Norris 2002). The short lag and observed brightness of the burst suggest that it is at a high redshift.

After a few hundred seconds, the prompt gamma-ray emission has decayed and the spectrum has softened to the point where high energy photons are no longer detectable. However, this late phase can often be detected in X-rays for many days after the initial burst as it was in GRB 050717. Several authors (Zhang et al. 2005; Nousek et al. 2005; Panaitescu et al. 2005) have presented a unified picture of the time evolution of the early X-ray emission and GRB 050717 fits this picture well. In this unified picture, the initial decay component has a steep time decay function where the emission is dominated by the tail of the internal shock emission (Kumar & Panaitescu 2000), followed by a shallower component where the fireball has decelerated and emission is dominated by the forward shock (Mészáros & Rees 1997; Sari, Piran, & Narayan 1998). The late decay of GRB 050717 is consistent with a steep decay from the tail of the internal shock emission superimposed on a less steep underlying afterglow component. At later times after the fireball has decayed, the emission is dominated by the forward shock component with an inferred X-ray flare, followed by a shallow decay.

GRB 050717 is a good example of a bright burst, possibly at high redshift, that exhibits many of the standard GRB features in both the prompt and afterglow light curves.

2. Observations and Data Analysis

The long GRB 050717 was detected by both the Burst Alert Telescope (BAT) (Barthelmy et al. 2005a) on Swift (Hurkett et al. 2005a) and the Konus instrument on WIND (Golenetskii et al. 2005), allowing simultaneous observations from 14 keV to 14 MeV. The burst was long enough that it was still detectable in Swift-BAT for >60 seconds after it became visible to the Swift X-Ray Telescope (XRT). The XRT continued to observe the afterglow until 7.1 days after the trigger and it was detectable out to 1.4 days. No optical transient was found in spite of deep long wavelength searches within 14 hours of the GRB.

2.1. Swift-BAT

At 10:30:52.21 UT, 17 July, 2005, the Swift BAT triggered and located on-board GRB 050717 (BAT trigger 146372) (Hurkett et al. 2005a). Unless otherwise specified, times in this article are referenced to the BAT trigger time, (UT 10:30:52.21) hereafter designated T_0. The burst was detected in the part of the BAT field of view that was 55% coded, meaning that it was 36° off-axis and only 55% of the BAT detectors were illuminated by the source. The spacecraft began to slew to the source location 8.66 seconds after the trigger and was settled

at the source location at T_0+63.46 seconds.

The BAT data for GRB 050717 between T_0-300 s and T_0+300 s were collected in event mode with 100 μs time resolution and ~6 keV energy resolution. The data was processed using standard Swift-BAT analysis tools and the spectra were fit using XSPEC 11.3. Each BAT event was mask-tagged using BATMASKWTEVT with the best fit source position. Mask-tagging is a technique in which each event is weighted by a factor representing the fractional exposure to the source through the BAT coded aperture. A weight of +1 corresponds to a fully open detector and a weight of -1 to a fully blocked detector. Flux from the background and other sources averages to zero with this method. All of the BAT GRB light curves shown have been background subtracted by this method. This method is effective even when the spacecraft is moving since complete aspect information is available during the maneuver.

The mask-weighting is also applied to produce weighted, background subtracted counts spectra using the tool BATBINEVT. Since the response matrix depends on the position of the source in the BAT field of view, separate matrices are derived for before the slew, after the slew and for individual segments of the light curve during the slew.

2.2. Konus-WIND

The long hard GRB 050717 triggered Konus-Wind (K-W) (Aptekar et al. 1995) at T_0(K-W) = 10:30:57.426 UT. It was detected by the S1 detector which observes the south ecliptic hemisphere; the incident angle was 55°.5. The propagation delay from Swift to Wind is 2.369 s for this GRB, *i.e.*, correcting for this factor, one sees that the K-W trigger time corresponds to T_0+2.86 s. The data before T_0(K-W)-0.512 s were collected in the waiting mode with 2.944 s time resolution. From T_0(K-W) to T_0(K-W)+430.848 s, 64 spectra in 101 channels were accumulated on time scales varying from 64 ms near the trigger to 7.17 s by the time the signal became undetectable. Data were processed using standard Konus-Wind analysis tools and the spectra were fitted by XSPEC 11.3. As observed by Konus-Wind GRB 050717 had a steep rise and a long decaying tail.

2.3. Swift-XRT

The spacecraft slewed immediately to the BAT location of GRB 050717 and the XRT began observing the burst at 10:32:11.49 UT (approximately 79 seconds after the BAT trigger). The automated on-board XRT software was unable to centroid on the burst, however, the downlinked X-ray spectrum and light curve clearly showed a bright fading X-ray object in the

field. XRT observations (Hurkett et al. 2005b) began in Windowed Timing (WT) mode (see below) 91 seconds after the trigger before going into Photon Counting (PC) mode at 310 s. The coordinates of the burst were determined by the XRT to be (J2000): RA:$14^h17^m24^s.58$ ($214^\circ.352$), Dec: $-50°31'59''.92$ ($-50^\circ.533$) (the 90% confidence error circle radius is 3.5 arc seconds) (Moretti et al. 2005).

Swift's X-ray Telescope uses a grazing incidence Wolter I telescope to focus X rays onto a CCD-22 detector. It has an effective area of 135 cm^2 at 1.5 keV and an angular resolution of 18 arcsec. For further information on the XRT see *e.g* (Burrows et al. 2003; Gehrels et al. 2004; Hill et al. 2004; Burrows et al. 2005a). This instrument has three key functions: the rapid, automated and accurate determination of GRB positions, the provision of moderate resolution spectroscopy (energy resolution 140 eV at 5.9 keV), and recording GRB light curves over a wide dynamic range covering more than seven orders of magnitude in flux.

The WT readout mode of the XRT uses a restricted portion of the telescope's total field of view: the central 8 arcmin (or 200 columns), when the GRB flux is below ~5000 mCrab. Each column is clocked continously to provide timing information with 1.8 ms resolution. However, this rapid readout mode only preserves imaging information in one dimension. Once the GRB flux drops below ~1 mCrab the PC mode takes over. This mode retains full imaging and spectroscopic information with a readout time of 2.5 s.

Data for this burst were obtained from the Swift Quick Look website [1] and processed with version 2 of the Swift software. The XSELECT program was used to extract source and background spectra and cleaned event lists (0.3–10.0 keV), using XSELECT grades 0–12 for PC mode data and grades 0–2 for WT data.

The PC mode suffers from pile-up when the count rate is ≥ 0.8 counts s^{-1}. To counter this we extracted a series of grade 0–12 background corrected spectra from the first 8.6 ks of PC mode data using annuli of varying inner radii. We deem the point at which pile-up no longer affects our results to be when the spectral shape no longer varies with an increase in annular radius. For GRB 050717 this occurred when we excluded the inner 12 pixels (radius). Only the first 500 s of PC mode data suffered from pile-up. The WT data were free from pile up problems. The spectra were then analyzed as normal in XSPEC 11.3.21. The light curve was created by the same method as detailed in Nousek et al. (2005).

[1] http://swift.gsfc.nasa.gov/cgi-bin/sdc/ql?

2.4. Swift-UVOT

The Swift Ultra Violet/Optical Telescope (UVOT) observations (Blustin et al. 2005) began at 10:32:10.7 UT (78 seconds after the BAT trigger). The first datum taken after the spacecraft settled was a 100 s exposure using the V filter with the midpoint of the observation at 128 s after the BAT trigger. No new source was detected within the XRT error circle in summed images in any of the six filters down to the 3σ magnitude upper limits shown in Table 1.

2.5. Other observations

GRB 050717 was not well positioned for follow-up observations. Its high southern declination made it unobservable by most northern hemisphere telescopes and the trigger was just before dawn at the South American observatories. Consequently, no follow-up optical observations were made until more than 13 hours after the burst. In the several observations that were made after this time, no optical counterpart was detected.

Under the control of Skynet, the Panchromatic Robotic Optical Monitoring and Polarimetry Telescopes (PROMPT) automatically observed the refined XRT localization of GRB 050717 beginning 13.0 hours after the burst (MacLeod et al. 2005). No source was detected within this localization. Limiting magnitudes (3σ), based on 5 USNO-B1.0 stars, are 21.7 (R_c, T_0+13.67 hr) and 21.5 (I_c, T_0+16.02 hr).

Observations in the K-band were made with the Wide-Field Infrared Camera on the du Pont 100-inch telescope at Las Campanas Observatory on two occasions: 2005 July 18.01 UT (T_0+13.7 hr) (Berger & Lopez-Morales 2005) and on 2005 July 18.98 UT (T_0+37.0 hr) (Berger et al. 2005). Within the 6′ radius XRT error circle four sources were found of which one is also visible in 2MASS K-band images. The other three sources have magnitudes of 18.1, 18.7, and 19.2 in comparison to several 2MASS stars; the 3σ limiting magnitude of the image is about 19.4. None of the three uncataloged objects faded between the two observations. In addition, Berger et al. (2005) obtained I-band images with the LDSS-3 instrument on the Magellan/Clay telescope on 2005 July 18.06 and 18.97 UT (14.9 and 36.8 hours after the burst, respectively). The same three sources visible in the K-band images were detected but had not faded.

Luckas, Trondal, & Schwartz (2005) obtained six five-minute unfiltered images on 2005 July 18.46 UT (24.5 hours after the burst), using one of Tenagra observatory's 0.35-m telescopes with an AP6 CCD at Perth, Western Australia. No new source was detected within the XRT error circle of GRB 050717 down to the DSS-2R limiting magnitude.

3. Light Curves and Spectroscopy

3.1. Swift-BAT

The BAT triggered on the first of two short, small spikes that preceded the main emission of GRB 050717. This first spike at T_0 was very soft (photon power-law spectral index 2.89 ± 0.14) and lasted 128 ms. The second short spike began at T_0+0.7 s, was of longer duration (320 ms) and was much harder (photon index 1.36 ± 0.23). The precursors are shown in detail in the left-hand panels of Fig 1. These small precursors were followed by the main pulse, which displayed the common fast rise, exponential decay (FRED) profile. The intensity rose from background to peak within 450 ms then began to decay with an average exponential decay constant $1.82^{+0.13}_{-0.11}$. The full light curve is shown in the right-hand panels of Fig 1. The peak count rate was measured by BAT to be ∼16000 counts s^{-1} at T_0+4 s in the 15-350 keV band. On top of this slow decay, there were at least four other peaks, showing a gradual spectral softening. The duration T_{90} (15–350 keV) is 86 ± 2 s (estimated error including systematics). The total fluence in the 15–350 keV band is (1.40 ± 0.03) $\times 10^{-5}$ erg cm^{-2}. The 1-s peak photon flux measured from T_0+2.8 s in the 15-350 band is 8.5 ± 0.4 ph cm^{-2} s^{-1}. All the quoted errors are at the 90% confidence level.

The BAT data were binned into eleven time bins to track the spectral evolution of the prompt emission. This is shown in the lower panels of Fig 1. Starting with the main peak, there is clear evidence of spectral softening as the burst progresses. Then after T_0+91 s, the BAT spectrum hardens again. The fit to the BAT data only over T_0+91 to T_0+150 s yields a power-law photon index of 1.08 ±0.32. A joint fit to the BAT and XRT data over the same time period (see Section 3.3) gives a photon index of 1.61 ± 0.08. The low BAT flux at these times limits statistically meaningful fits to the entire interval. However, given the spectral variation demonstrated earlier in the burst, it is quite possible that there is spectral evolution occurring at these times as well and the overall spectral fits should be interpreted with caution.

3.2. Konus-WIND

The Konus-Wind light curve is shown in three energy bands in Fig 2, and the 21–1300 keV light curve (see Fig 3) is similar to the Swift-BAT light curve. The long decaying tail is clearly seen in G1 band (21–84 keV), marginally seen in G2 band (84–360 keV), and not seen in G3 band (360–1370 keV). The G2/G1 ratio demonstrates substantial softening of the tail as compared to the main pulse. The T_{90} durations of the burst in G1, G2, G3 energy bands are 99±10 s, 95±11 s, 18±3 s, respectively. For the sum G1+G2+G3, the T_{90}

duration is 96±6 s.

Emission is seen up to ∼6 MeV. The spectrum of the main peak (from T_0+2.843 s to T_0+8.219 s) is well fitted (in the 20 keV–10 MeV range) by a power law model with an exponential cutoff: $F(E) = A \times (E/100\ \mathrm{keV})^{-\alpha} \times \exp\left(\frac{-E(2-\alpha)}{E_{peak}}\right)$, where E is the energy in keV, E_{peak} is the peak energy of the $\nu \times F(\nu)$ spectrum, α is the photon index, and A is a normalization factor. In this fit, $\alpha = 1.05 \pm 0.10$ and $E_{peak} = 2250^{+940}_{-620}$ keV (χ^2= 83 for 85 d.o.f.). Fitting jointly with the BAT data gives $\alpha = 1.04 \pm 0.05$ and $E_{peak} = 2401^{+781}_{-568}$ keV (χ^2= 117 for 143 d.o.f.). Figure 4 shows that the BAT and Konus data can be well fit to the same model spectrum. A fit to the Band (GRBM) model was also attempted. No statistically significant high energy power-law tail was established. The limit on the high energy photon index is $\beta > 1.89$ (90% C.L.) The low energy photon index α is almost the same as for the cut-off power-law model, $\alpha = 1.02^{+0.7}_{-0.3}$. Joint fits between BAT and Konus were also made for two later time intervals: T_0+13.851 s – T_0+26.907 s, and T_0+26.907 s – T_0+54.555 s. The photon indices for a simple power-law fit are shown in Figure 1. The first of these intervals was also fit with a cut-off power law, but only a lower limit to E_{peak} was found: $E_{peak} > 548$ keV (90% C.L.)

The total fluence in the 20 keV to 6 MeV range is $6.5^{+0.9}_{-2.2} \times 10^{-5}$ erg cm^{-2}. The 64-ms peak flux measured from T_0+2.86 s in the same energy band is $1.41^{+0.18}_{-0.24} \times 10^{-5}$ erg cm^{-2} s^{-1}. The uncertainties in the derived fluence and peak flux are dominated by uncertainties in the high energy part of the spectrum.

All quoted uncertainties are at the 90% confidence level.

3.3. Swift-XRT

The spectrum between 91 s and 310 s after the trigger (WT data) has an average photon index of 1.65 ± 0.11, with the absorption fixed at its galactic value of 2.22×10^{21} cm^{-2} and an indication of an excess absorption of $2.75 \pm 0.57 \times 10^{21}$ cm^{-2} , assuming $z = 0$ and standard (local) interstellar material abundances. The mean unabsorbed flux in WT mode at 201 s (mean time) is $5.76 \pm 0.31 \times 10^{-10}$ erg cm^{-2} s^{-1} in the 0.3-10.0 keV energy range.

During the period between T_0+91 s and T_0+150 s, a joint fit was made to the XRT and BAT data. The joint fit gives a photon index of 1.61 ± 0.08, with an excess absorption of $3.36^{+0.8}_{-0.68} \times 10^{21}$ cm^{-2} ($\chi^2 = 125$ for 115 d.o.f.). This fit was used to extrapolate the BAT 15-150 keV flux into the XRT energy range (0.3–10 keV) during the overlap interval assuming that the 1.61 power law index holds in both energy ranges. Since we know the BAT count rate in the BAT (15–150 keV) range, we were able to use XSPEC to derive the model flux

in the 0.3-10 keV band and then calculate a ratio between BAT counts (15–150 keV) and flux (0.3–10 keV). For earlier epochs we derived the conversion ratio from the model fits to the BAT data alone. We derived a similar ratio between XRT counts (0.3–10 keV) and flux. With this extrapolation one can directly compare the early and later light curves and show (Figures 5 and 6) that the prompt emission smoothly transitions to the afterglow emission.

The data from T_0+1.17 hr to T_0+8.25 hr were also fit with a power law with a photon index of 1.35±0.21 and galactic absorption (χ^2=16.9 for 11 d.o.f.). The model flux over 0.3–10.0 keV was 1.8±0.41 $\times 10^{-12}$ ergs cm^{-2} s^{-1} ($3.54^{+0.89}_{-1.00} \times 10^{-4}$ photons cm^{-2} s^{-1}). In this case there was no improvement to the fit by adding excess absorption. Indeed, this later spectrum is not consistent with excess absorption at the level implied by the earlier WT data; the excess absorption is limited at 90% confidence to $< 1.5 \times 10^{21}$ cm^{-2}.

3.4. Post-Burst Emission

The gamma-ray and X-ray decay light curve is shown in Fig 5. The light curve shows several prominent features which can be interpreted in light of the models discussed in Zhang et al. (2005) (hereafter Z05). First, as pointed out earlier there is a smooth transition from the prompt BAT emission into the early X-ray emission and a fairly steep decay (power law index α_1 in the discussion below) until $T_0 > \sim 200$ s. This is followed by a possible superimposed X-ray flare, a phenomenon quite common in GRBs as observed by Swift (Burrows et al. 2005b; Barthelmy et al. 2005b). Unfortunately observing constraints cut off observations in the middle of the possible flare, and the statistics do not allow for a meaningful fit to a flare component. Observations resumed again at T_0+ 4214 s, with a return to a power-law decay, with a shallower power law index (α_2 below).

In order to fit the data to reasonable X-ray emission models, two intervals were removed: BAT data points before T_0+ 50 s, which were believed to be part of the prompt emission, and XRT data points between T_0+500 and the end of the first observation, so that the fit is not contaminated by the possible flare. Three different fits were made and are discussed in turn.

First, we tried a broken power law. This gave a power law index $\alpha_1 = 2.10^{+0.17}_{-0.05}$ for the steep part of the light curve, a break time of 203 ± 26 s and an index $\alpha_2 = 1.48 \pm 0.02$ for the shallow part ($\chi^2 = 159$ for 111 d.o.f.). The steep part of the curve ($\alpha_1 = 2.10$) corresponds to region I in Fig. 1 of Z05. According to Z05, if this time can be interpreted as the curvature effect (Kumar & Panaitescu 2000; Dermer 2004), the index should be $\alpha = 2 + \beta$, where β is the *energy* index of the spectrum of the emission. Taking $\beta = 0.62$, we should have $\alpha_1 =$

2.62, as compared to the observed value of 2.10.

One factor which could lead to a deviation from the $\alpha = 2+\beta$ relation is that the decay curve seen could be a superposition of two separate decay power laws, one steep due to the curvature component, and one shallow due to the forward shock component. So a fit was made to a superposition model: $F(t) = A \times t^{-\alpha_1} + C \times t^{-\alpha_2}$, where A and C are normalization factors. This fit gave a steep index $\alpha_1 = 3.01^{+0.55}_{-0.23}$ and a shallow index $\alpha_2 = 1.43 \pm 0.04$ ($\chi^2 = 161$ for 110 d.o.f). Statistically this fit is indistinguishable from the broken power law. However the physical interpretation is more straightforward. The steep index ($\alpha_1 = 3.01$) is the decay of the tail of the internal shock emission, which is superimposed on an underlying afterglow component with a decay index of $\alpha_2 = 1.43$. The afterglow component becomes dominant at $T_0+ \sim 100$ s.

An alternative model is that one of the peaks seen in the light curve near $T_0+ \sim 50$ s is the onset of the external shock. To test this hypothesis, we performed a fit to a single power law, but allowed the time of the start of the afterglow to be a free parameter: $F(t) = A \times (t - t_0)^{-\alpha}$, where A is the normalization. This fit gave $t_0 = 28.8 \pm 2.4$ s and $\alpha = 1.44 \pm 0.02$ ($\chi^2 = 171.7$ for 111 d.o.f.) This decay index is consistent with the late time decay index in the other two fits and gives further credence to the idea that we are seeing the influence of the external shock throughout the afterglow light curve. However, there is no statistical reason to favor this model over the other two. In fact χ^2 is somewhat larger for the single power law model. Kobayashi et al. (2006) have derived a rough relationship between t_0 and the onset of the afterglow; using this relationship, we predict that the afterglow should have begun at $T_0+ \sim 40$ s, consistent with a peak seen in the light curve.

It is instructive to compare the measured temporal index ($\alpha_2 \approx 1.4$) with the values predicted by the simple afterglow models compiled by Zhang & Mészáros (2004). At late times (t >1.17 hr), we should be in the slow cooling regime, and the spectral index of GRB 050717, $\beta = 0.35 \pm 0.21$, is consistent only with the regime where $\nu_m < \nu < \nu_c$. Here, following Zhang & Mészáros (2004), ν is the spectral frequency of the emission, and ν_m and ν_c are the synchotron frequency and cooling frequency, respectively. Using $\beta = 0.35 \pm 0.21$, we have the electron-acceleration power-law index $p = 1+2\beta = 1.7 \pm 0.4$. Using the equations in Table 1 of Zhang & Mészáros (2004) [2] and taking $p > 2$, we derive values for α of 0.5 ± 0.3, and 1.0 ± 0.3 for the ambient interstellar medium (ISM) (Mészáros & Rees 1997; Sari, Piran, & Narayan 1998) and wind models (Chevalier & Li 2000), respectively. If $1 < p < 2$, we derive α values of 0.7 ± 0.1, 1.2 ± 0.05, again for the ISM and wind models, respectively.

[2]We have changed the signs of α and β in the equations of Zhang & Mészáros (2004) to conform to the definition $F_\nu \propto t^{-\alpha} t^{-\beta}$ used in this paper.

We see that the late-time temporal index ($\alpha_2 \approx 1.4$) is inconsistent with the ISM model and marginally consistent with the wind model. This analysis shows that at late times emission is dominated by the forward shock with a wind density profile.

In order for the afterglow of GRB 050717 to have $\nu_m < \nu < \nu_c$, it must be observed at a time such that $t > t_c$, where the critical time t_c is defined in Z05. This puts constraints on the wind parameter A_*, which is defined in (Chevalier & Li 2000) as being proportional to the wind mass loss rate divided by the wind velocity (units g cm^{-1}). The parameter A_* must be in the range 0.01–0.001, which is similar to the limit derived for GRB 050128 (Campana et al. 2005).

The late time shallow decay (index ~ 1.4) continues until the flux becomes unobservable to the XRT. A lower limit is set for summed observations after T_0+2.6 days. Since there is no apparent break to a steeper decay in the light curve, the lower limit on a jet-break time is $t_b > 1.4$ days.

4. Discussion

4.1. Spectral Lag

It is possible to derive an estimate of the spectral lag of the BAT data between Channel 1 (15-25 keV) and Channel 4 (100–350 keV). From the spectral lag we can use the methodology of Norris, Marani, & Bonnell (2000) and Norris (2002) to derive limits on the redshift of the GRB and on the isotropic luminosity of the peak of the emission. The spectral lag was derived for the main peak of emission (from T_0+2.26 s to T_0+5.8 s). The lag was found to be $2.5^{+2.9}_{-2.4}$ ms. Hence the measured lag is statistically consistent with zero. The lag was also measured for several other intervals during the burst and with time rebinning ranging from 2 ms to 16 ms. In all cases, the measured lag was small, positive and consistent with zero. Such a low value for lag is quite unique for a long burst since Norris (2002) has shown that the dynamic range of lags for long bursts spans $\sim$ 25 ms to $\sim$ 300 ms. In fact out of the 90 brightest bursts studied by Norris (2002), only 2% show a lag as small as that of GRB 050717.

One can use the lag, the measured peak flux, and E_{peak} to set lower limits on the distance to burst. Using the peak flux of $1.69 \pm 0.16 \times 10^{-6}$ ergs cm^{-2} s^{-1} (15–350 keV; T_0+2.752 s to T_0+3.008 s), the parameters from the joint Konus-BAT fits to the main peak (Section 3.2) and the $+2\sigma$ limit on the lag (8.3 ms), one derives a redshift of 2.7 and a peak luminosity of 3.9×10^{53} ergs s^{-1} (15–350 keV). The fit is relatively insensitive to variations in either peak flux or E_{peak} and other spectral fit parameters. Since smaller values of spectral lag would lead

to larger redshifts, this value, z = 2.7, can be considered the 2σ lower limit on the redshift; similarly the luminosity is also a lower limit. Such a large redshift is consistent with the non-detection of an optical or infrared counterpart to the afterglow (Sections 2.5 and 4.2) and with the non-detection of a jet break (Section 3.4). The corresponding lower limits on the isotropic radiated energy, the isotropic peak luminosity (both 20–6000 keV), and peak energy in the source rest frame are $E_\gamma^{iso} > 1.0 \times 10^{54}$ ergs, $L_{max}^{iso} > 8.7 \times 10^{53}$ erg s^{-1}, and $E_{peak}^{rest} > 8900$ keV (for a standard cosmology: $\Omega_M = 0.3$, $\Omega_\Lambda = 0.7$, $H_0 = 70$ km s^{-1} Mpc^{-1}).

A consistent interpretation of such a small lag is that the high energy emission from GRB 050717 has been redshifted downward more than usual into the BAT energy range. It has been shown (Norris et al. 1996; Fenimore & Bloom 1995) that the high energy component of burst emission shows narrower peaks and more variation than is seen at lower energies. Shifting such spiky peaks into the BAT range would cause the measured lag to be smaller than what would be observed in long bursts at lower redshifts.

Norris & Bonnell (2005) have pointed out that many short bursts seen by BATSE, Swift, Konus-Wind, and HETE-2 have extended emission starting a few seconds after the short spike and lasting for ∼tens of seconds. Since short bursts are also known to have short lags (Norris, Scargle, & Bonnell 2001), is it possible that GRB 050717 is in fact a short burst? This burst has a pair of precursors of duration 128 ms and 320 ms, followed by > 100 s of extended emission along with a spectral lag consistent with short GRBs. However, two properties of GRB 050717 argue strongly against it being a short burst. First of all, the spectra of the precursors of this burst are significantly softer than the extended emission (see Fig 1), while in all short bursts with extended emission the short spikes are significantly harder than the extended emission. Secondly, in GRB 050717, the flux is dominated by the extended emission, while in short bursts, the flux is dominated by the short episode of emission. Therefore, it is more likely that GRB 050717 is indeed a long burst seen at a large distance.

Using a relationship derived by Liang & Zhang (2005) we can use the measured E_{peak} and the limits on luminosity and redshift to set a lower limit on the jet break time for this burst. After re-arranging Equation 5 in Liang & Zhang (2005):

$$t_b = 0.88 \times (E_{\gamma,iso,52})^{-0.81} \times \left(\frac{E_p}{100keV}\right)^{1.56} \times (1+z)^{2.56}. \quad (1)$$

Here t_b is the jet break time in days in the observer frame, $E_{\gamma,iso,52} > 100$ is the isotropic energy in units of 10^{52} ergs and E_p=2400 keV is the observed peak energy. Errors on the exponents in the equation have been suppressed since the calculation is dominated by errors

in the input parameters. With these values and z=2.7, we can derive a lower limit on t_b of 88 days. As we saw in Section 3.4 this is fully consistent with the observations.

4.2. Lack of Optical Counterpart

As noted in Sections 2.4 and 2.5, no optical counterpart to GRB 050717 was found. The deepest limits were those obtained from PROMPT, at 21.7 (R_c, T_0+13.67 hr) and 21.5 (I_c, T_0+16.02 hr). What conclusions can be drawn from the lack of an infrared counterpart?

First of all, is GRB 050717 a dark burst? Jakobsson et al. (2004) make a comparison between the observed X-ray flux and the R-band magnitude of the afterglow at ten hours after the trigger for a large set of bursts and define a dark burst as a burst lying in a certain region of the log(F_{opt})-log(F_X) diagram. For GRB 050717, the X-ray flux interpolated to T_0+10 hr is 0.015 μJy (see Figure 5) and the R-band limit extrapolated to T_0+10 hr would be $R_c \approx 21.5$. This is solidly within the bright burst region of the Jakobsson et al. (2004) diagram; thus it is not possible to say that this is a dark burst given how late the optical limits are.

Similarly the lack of a counterpart cannot be used as confirmation of the high redshift. Assuming $z = 2.7$, the Lyman edge would be redshifted to 91.2 nm$(z + 1) = 337$ nm. This is consistent with the relatively shallow ultraviolet limits set by UVOT, but the counterpart could still easily be observed in the I band. It is instructive to compare the infrared observations of GRB 050717 to those of GRB 050904, a high redshift ($z = 6.29$) burst for which an infrared counterpart was found. However, the IR observations of GRB 050904 were either much earlier (J$\sim$ 17.5, $T_0+ \sim$ 3 hr) (Haislip et al. 2005) or much deeper (I$\sim 22.9 \pm 0.6$, $T_0+ \sim$ 37 hr) (Perley et al. 2005) than those obtained for GRB 050717. The lack of an observed counterpart to GRB 050717 must be attributed to the lateness of the observations.

5. Conclusions

The long gamma-ray burst GRB 050717 shows a number of interesting features which can be interpreted in light of the predominant models of bursts and their afterglows. First of all the short spectral lag tells us that this burst is at a high redshift ($z > 2.7$) and hence has a large intrinsic luminosity ($L_{peak} > 8.7 \times 10^{53}$ erg s^{-1}). The features observed in the burst are likely representative of spiky high energy features red-shifted to the BAT energy range.

The main emission of the burst clearly exhibits hard to soft spectral evolution as dis-

cussed in Zhang & Mészáros (2004) and Norris et al. (1986). The light curve of the prompt emission (Fig 1) begins with two short, faint, spectrally soft spikes, followed by an intense peak which is the hardest portion of the burst. The burst intensity envelope as seen above 15 keV decays over the next $\sim$ 150 seconds until it becomes detectable only at lower energies. Superimposed on the overall decay are at least four subsidiary peaks, each of which is less intense and softer than the one before. However the spectra of the peaks are harder than the intervening valleys. Furthermore, as seen in Figs 1 and 3, each peak is time-asymmetric at all energies. Thus the time profile of this burst is a very good example of the overall time asymmetry described by Nemiroff et al. (1994).

GRB 050717 also demonstrates many of the features of the unified picture of the late time evolution of GRB emission (Zhang et al. 2005; Nousek et al. 2005; Panaitescu et al. 2005). When the BAT flux is extrapolated to the 0.3–10 keV energy range it is seen that the prompt emission smoothly transitions into the slowly decaying phase. During the early X-ray emission of GRB 050717, the decay index is somewhat less steep than would be expected if it were due solely to the tail emission of the prompt GRB. As discussed in Section 3.4, this can be interpreted as a superposition of tail and external shock emission, although other interpretations are also discussed. The decay trend is consistent with the onset of the afterglow occurring at $T_0+ \sim 45$ s. Before data collection was cut off by an orbital constraint at $\sim$ 800 s after the trigger, the light curve shows evidence of the start of an X-ray flare, When observations take up again, the flux is much weaker and the decay index is shallow, since at this time the afterglow is dominated by the forward shock. The flux became too faint to observe before the expected jet break at $t_b > 90$ days.

Most of the burst and afterglow properties are common and easily interpreted. This is an indication that these properties also hold for bright, high redshift bursts.

HAK was supported in this work by the Swift project, funded by NASA. This work is supported at the University of Leicester by the Particle Physics and Astronomy Research Council (PPARC). CPH gratefully acknowledges support from a PPARC studentship. The Konus-Wind experiment is supported by Russian Space Agency contract and RFBR grant 03-02-1751. HAK is also grateful for useful discussions with T. Sakamoto and P. O'Brien.

REFERENCES

Band, D.L., 1997, ApJ,486, 928

Band, D.L. & Ford, L. 1998, Advances in Space Research, 22, 1093

Aptekar, R.L. et al., 1995, Space Sci. Rev.,71, 265

Barthelmy, S. et al., 2005a, Space Sci. Rev. in press (astroph/0507410)

Barthelmy, S. et al., 2005a, Nature in press

Berger, E. &. Lopez-Morales, M., 2005, GCN Circ 3639

Berger, E. et al., 2005, GCN Circ 3643

Blustin, A. et al, 2005, GCN Circ 3638

Burrows, D. N. et al. 2003, Proc. SPIE, 5165, 201-216.

Burrows, D.N. et al., 2005a, Space Sci. Rev. in press (astroph/0508071)

Burrows, D.N. et al., 2005b, Science, 309, 1833

Campana, S. et al, 2005, ApJ, 625, L23

Chevalier, R.A., & Li, Z-Y, 2000, ApJ, 536, 195

Dermer, C. D., 2004, ApJ, 614, 284

Fenimore, E.E. & Bloom, J. S., 1995, ApJ, 453, 25

Gehrels, N. et al., 2004, ApJ, 611, 1005

Golenetskii, S. et al, 1983, Nature306, 451

Golenetskii, S. et al, 2005, GCN Circ 3640

Haislip, J. et al, 2005, GCN Circ 3913

Hill, J.. et al, 2004, SPIE 5165, 217

Hurkett, C. et al, 2005a, GCN Circ 3633

Hurkett, C. et al, 2005b, GCN Circ 3636

Jakobsson, P., et al., 2004, ApJ, 617, L21

Kobayashi, S. et al., 2006, in preparation

Kumar, P. & Panaitescu, A., 2000, ApJ, 541, L51

Liang, E. & Zhang, B., 2005, ApJ, 633, 611

Luckas, P. , Trondal, O., & Schwartz, M., 2005, GCN Circ 3642

MacLeod, C.. et al, 2005, GCN Circ 3652

Mészáros, P. & Rees, M., 1997, ApJ, 476, 232

Moretti, A., et al. 2005, A&A in press (astroph/0511604).

Nemiroff, R.J., et al. 1994, ApJ, 423, 432

Norris, J.P., et al. 1986, ApJ, 301, 213

Norris, J.P., et al. 1996, ApJ, 459, 393

Norris, J.P., Marani, G.F., & Bonnell, J.T., 2000, ApJ, 534, 248

Norris, J.P., Scargle, J.D., & Bonnell, J.T., 2001, *Proceedings of Rome 2000 Gamma-Ray Bursts in the Afterglow Era*, eds. E. Costa, F. Frontera, & J. Hjorth (Heidelberg: Springer), p. 40

Norris, J.P., 2002, ApJ, 579, 386

Norris, J.P. & Bonnell, J.T., 2005, ApJ submitted.

Nousek, J. A. et al. 2005, ApJ in press (astroph/0508332).

Panaitescu, A., Mészáros, P., Gehrels, N., Burrows, D., & Nousek, J. 2005, MNRAS in press (astroph/050840).

Perley, D. et al, 2005, GCN Circ 3932

Sari, R., Piran, T., & Narayan, R., 1998 ApJ, 497, L17

Zhang, B., & Mészáros, P., 2004, International Journal of Modern Physics A ,19, 2385

Zhang, B., et al., 2005, astro-ph/0508321

This preprint was prepared with the AAS LaTeX macros v5.2.

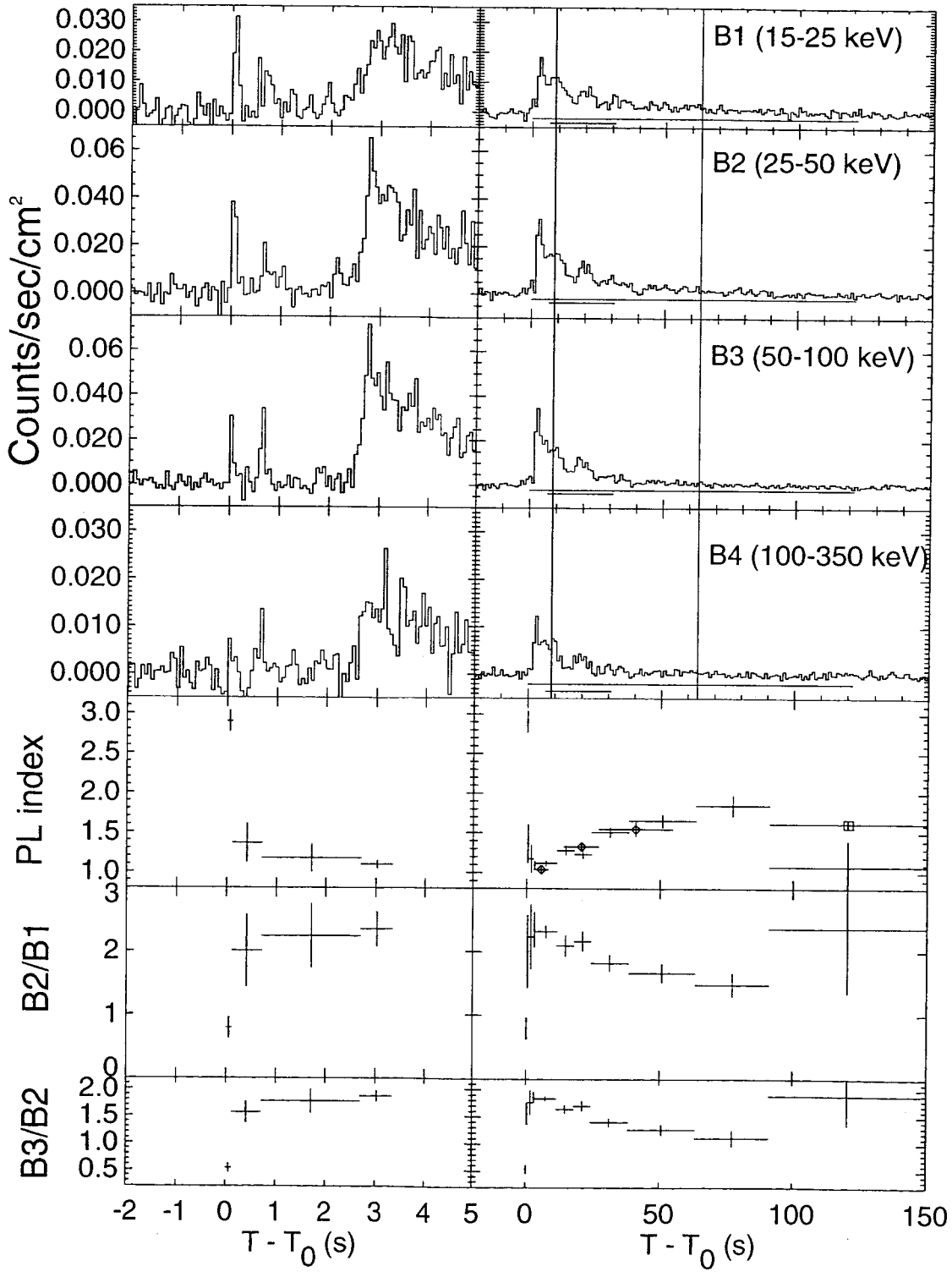

Fig. 1.— See next page for caption.

Fig. 1. – Background subtracted BAT light curves, power-law fit indices and hardness ratios for GRB 050717. The panels on the right show the full duration of the prompt emission; those on the left zoom in to show the precursor peaks in the light curves more clearly. **Light curves (top four sets of plots):** The rate is corrected for the effective area as a function of source location in the field of view before and during the slew. After the slew the source is on-axis. The start and end of the slew to the target are shown by vertical lines. The burst duration measures T_{90} and T_{50} are shown by horizontal lines in the right hand plots, with T_{90} shown above T_{50}. The time binning is 1 s for the right-hand plots and 64 ms for those on the left. **Power Law fit photon index (fifth set of plots):** Separate fits were made to each time interval indicated. The BAT data (plain symbols) are best fit by a simple power law. The plot also shows joint fits to the BAT and Wind data (open diamonds) and to the BAT and XRT data (open square). For the leftmost BAT/Wind point, the index α of the cut-off power law fit (see text) is shown. For the other joint fit points, the photon index from a power-law fit is shown. **BAT hardness ratios (lower two sets of plots):** Two sets of ratios (defined on the plot) are shown to illustrate the spectral hardening during the rise to the main peak, followed by a softening as the prompt emission evolves. The final data points show a second hardening of the spectrum. The time scale is the same for all plots in a vertical column.

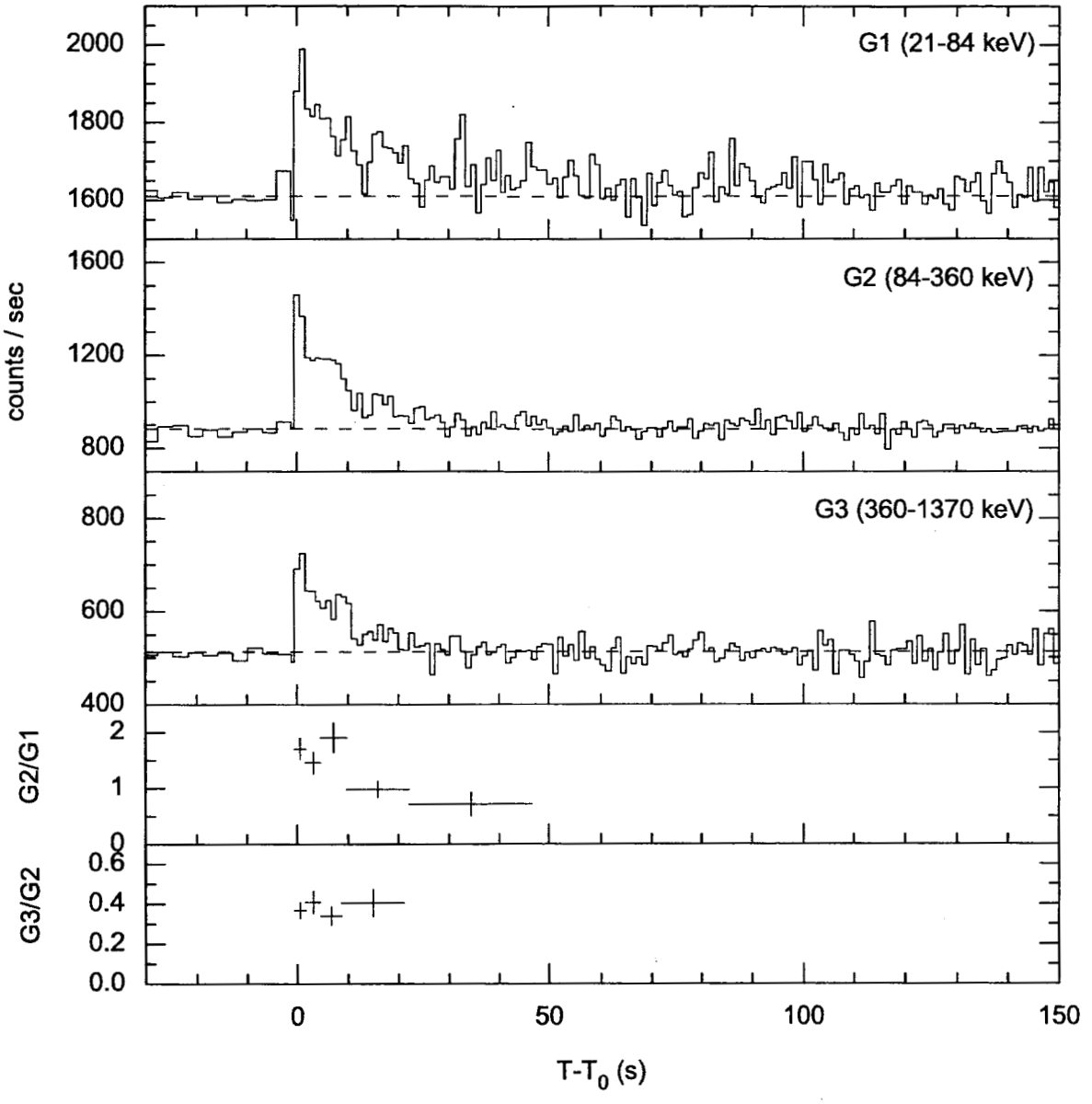

Fig. 2.— The Konus-WIND light curve for GRB 050717 in three energy bands. The data before T-T_0(K-W) =-0.512 s were recorded in the waiting mode with 2.944-s time resolution, after that data were recorded at finer time resolution and binned at 1.024 sec. The energy bands used in the hardness ratios at the bottom of the plot are defined in the top panels of the plot.

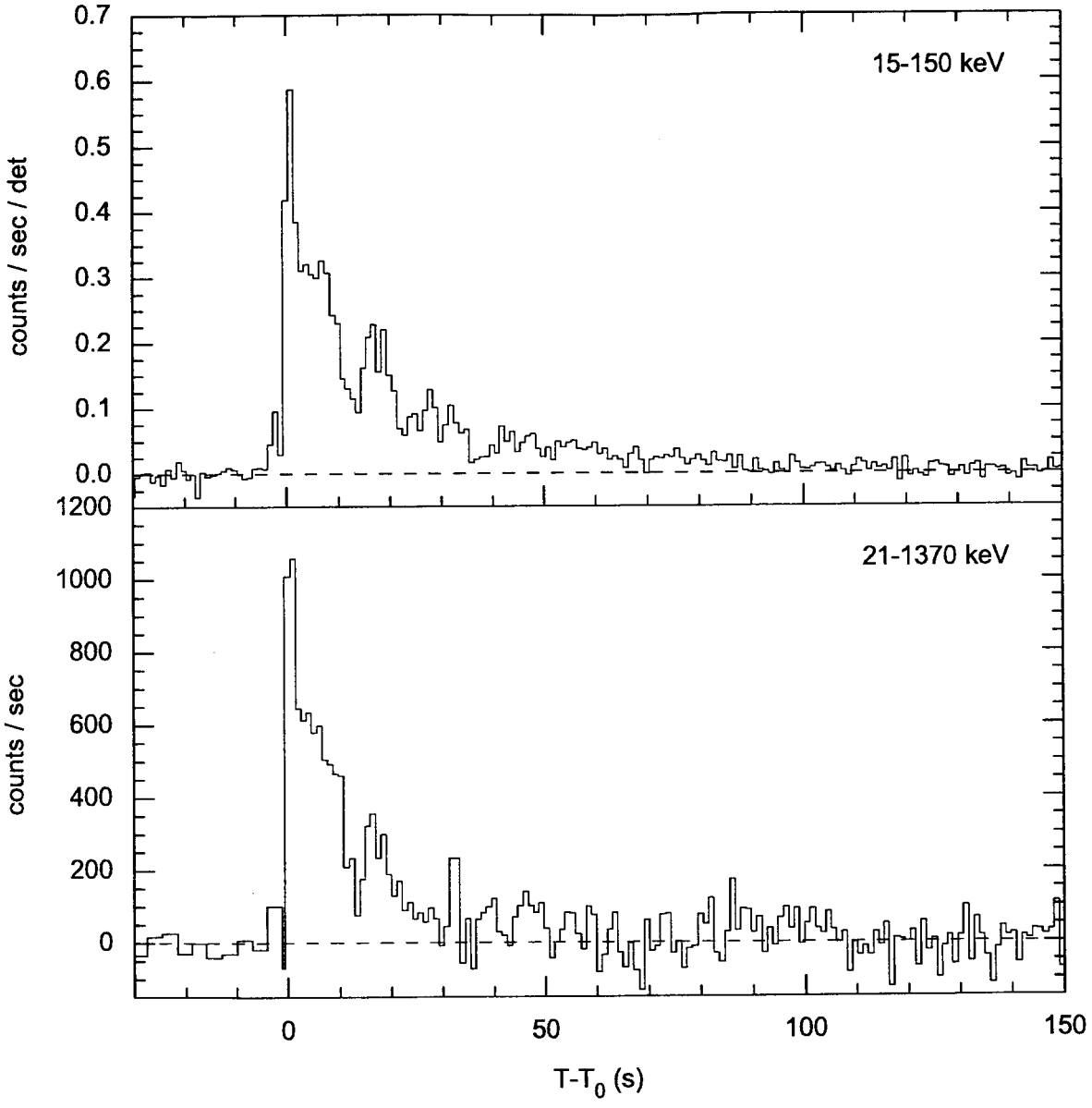

Fig. 3.— The background subtracted BAT (top panel) and Konus-WIND (bottom) light curves on the same time scale. The plots have been adjusted so that the trigger time for both plots are the same relative to the burst. This means that T_0 in the lower plot is actually T_0(BAT) plus the propagation time between the spacecrafts (2.369 s).

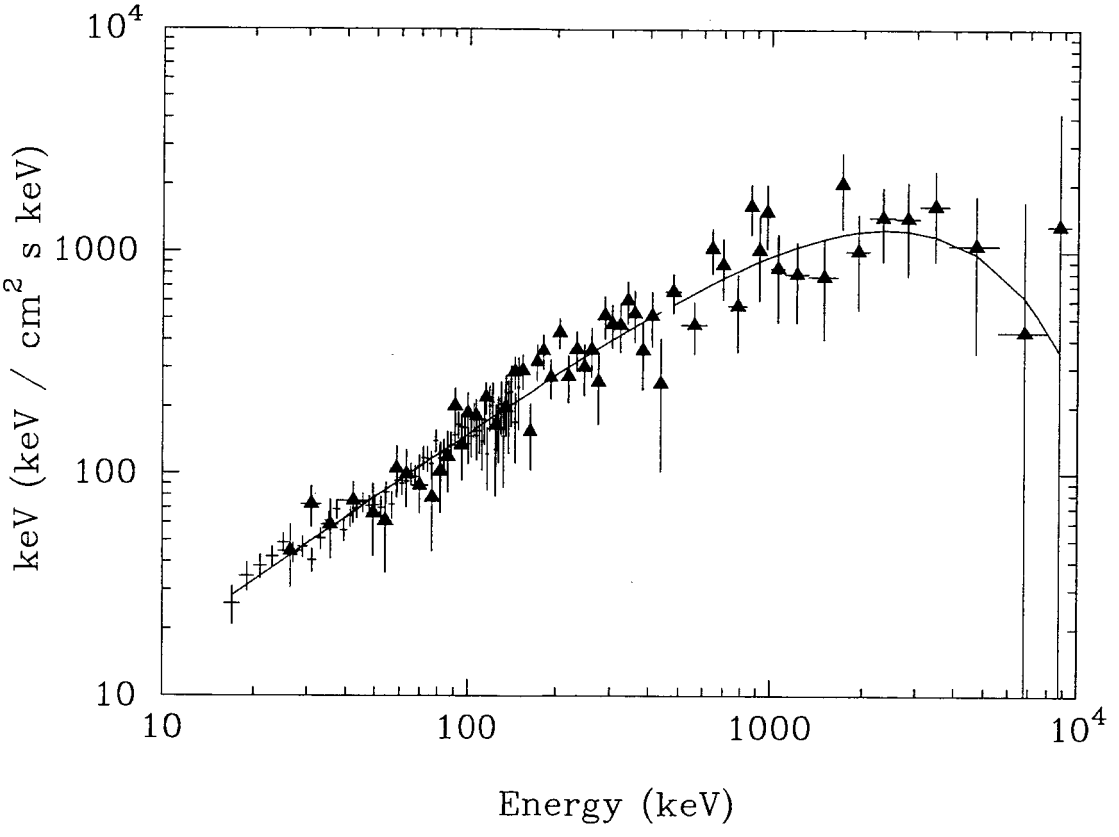

Fig. 4.— Joint fit to a cut-off power law model (defined in the text) for the BAT and Konus-Wind data during the main peak of emission T_0+2.843 s to T_0+8.219 s. The value of E_{peak} for this fit is 2401^{+781}_{-568} keV. Points from the BAT spectrum are shown as crosses, those from the Konus spectrum are shown as filled triangles.

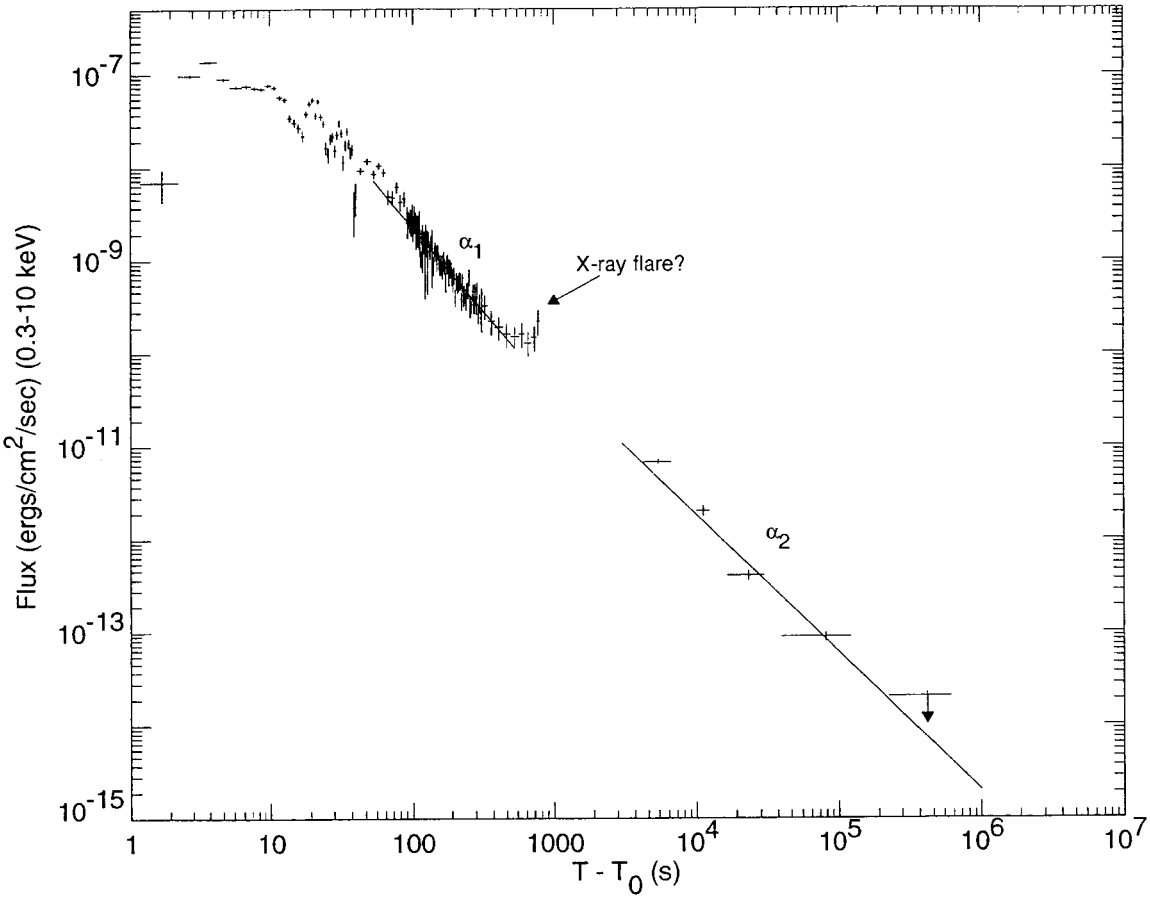

Fig. 5.— The combined BAT prompt emission and XRT afterglow light curve. Points in the BAT light curve have been extrapolated from the BAT 15–150 keV energy band to the XRT 0.3–10 keV band and corrected for differences in the effective area (see discussion in the text). This shows how the prompt emission makes a smooth transition into the afterglow. The broken power law fit to the X-ray light curve decay is also shown ($\alpha_1 = 2.10; \alpha_2 = 1.48$). The last data point (upper limit) was combined from five orbits in PC mode.

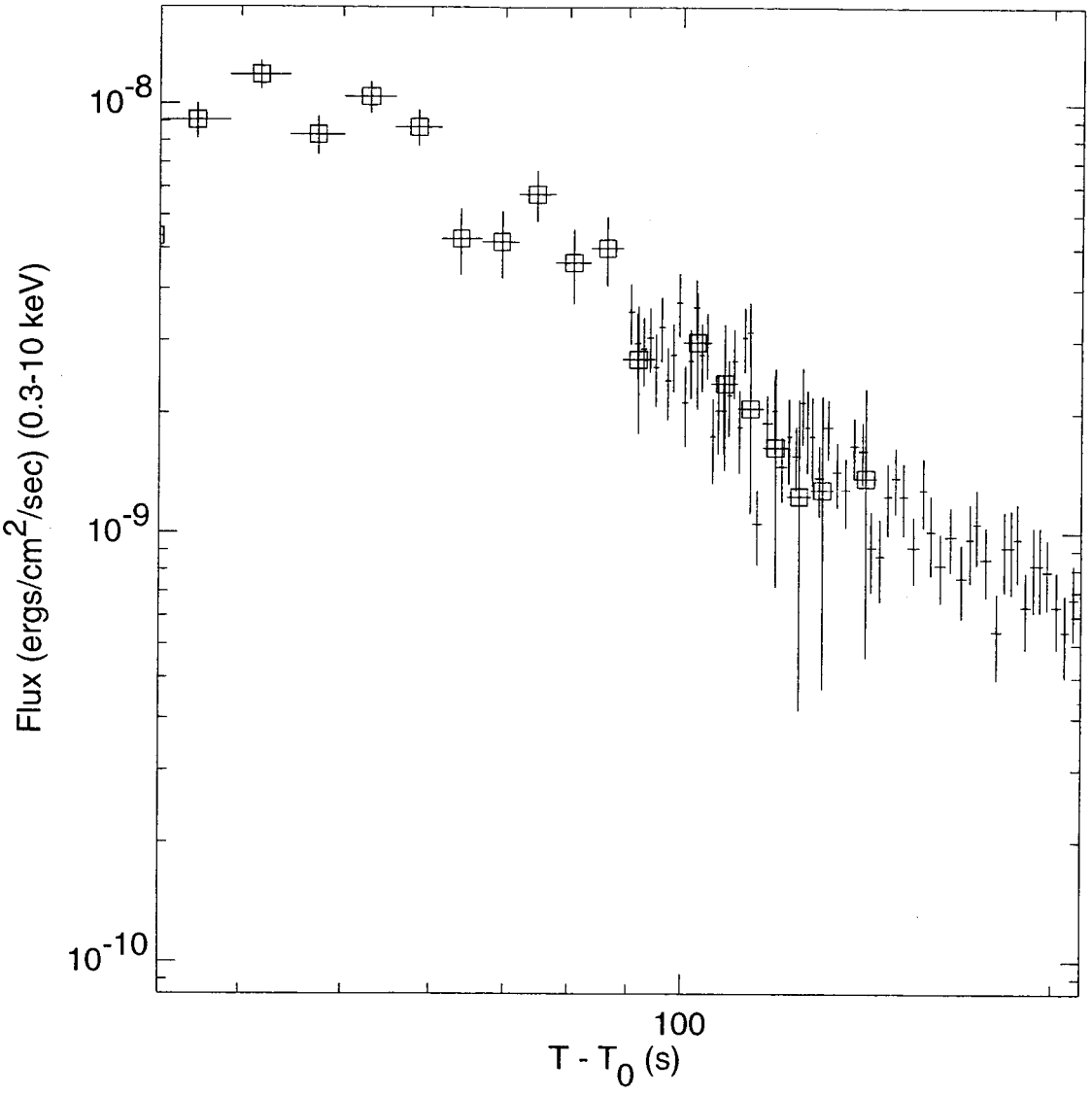

Fig. 6.— The section of Figure 5 showing the overlap between BAT (open squares) and XRT (crosses) emission. This figure clearly shows the smooth transition from prompt gamma-ray to early X-ray emission. See caption to Figure 5 and the text for a discussion of the extrapolation of the BAT data points.

Table 1. UVOT Limiting magnitudes

Filter	Exposure (s)	T_{mid} (s)	3-sigma limit
V	168	424	19.00
B	75	524	19.59
U	78	511	19.34
UVW1	78	498	18.62
UVM2	78	483	18.79
UVW2	68	498	18.73

Note. — Data taken from GCN 3638 (Blustin et al). T_{mid} is the mid-point of the summed observation measured with respect to the BAT trigger time T_0.